Desalination and Water Treatment
www.deswater.com

doi: 10.5004/dwt.2020.24894

174 (2020) 248–257
January

Advanced oxidative process by heterogeneous photocatalysis for chemical laboratories effluents treatment

Carlos Antônio Pereira de Lima[a,*], Bruna Aline Araujo[a], Karyna Steffane da Silva[a], Camylla Barbosa Silva[a], Geralda Gilvânia Cavalcante de Lima[a], Fernando Fernandes Vieira[a], Keila Machado de Medeiros[b]

[a]*Sanitary and Environmental Engineering Department, State University of Paraíba, Av. Baraúnas, 351, 58429-500, Campina Grande, Paraiba, Brazil, Tel. +55 83 3315 3333; emails: caplima@uepb.edu.br (C.A.P. de Lima), brunaaaraujo15@gmail.com (B.A Araujo), karynasteffane@hotmail.com (K.S. da Silva), camyllabsilva@hotmail.com (C.B. Silva), gilvania@uepb.edu.br (G.G.C. de Lima), fernando@uepb.edu.br (F.F. Vieira)*

[b]*Science and Technology Center in Energy and Sustainability, Federal University of Recôncavo da Bahia, Av. Centenário, 697, Sim, 44042-280, Feira de Santana, Bahia, Brazil, Tel. +55 75 3622 9351; email: keilamedeiros@ufrb.edu.br*

Received 17 April 2019; Accepted 11 September 2019

ABSTRACT

In this article, a solution of methylene blue (MB) was submitted to a photocatalytic process, was used as the basis for studies of more complex compounds such as the effluents from universities' laboratories. MB is a standard compound for many photocatalytic tests. The use of commercial titanium dioxide (TiO_2) in degradation of toxic compounds is very suitable as it is a cheap and effective. Therefore, its characterization confirmed that its physicochemical properties fit this purpose. TiO_2 particles were characterized by X-ray fluorescence (XFR), X-ray diffraction (XRD), Fourier transform infrared spectroscopy (FTIR), scanning electron microscopy (SEM) and particle size analysis. The chemical composition of titanium dioxide by XFR was 98.6% pure. Through XRD, it was possible to realize that TiO_2 presented the anatase and rutile crystalline phases, with predominance of the anatase phase. By FTIR, two TiO_2 characteristic bands were found at 505 and 612 cm^{-1}. By SEM, it was visualized that TiO_2 had a structure with uniformly distributed spherical particles. The particle size distribution of TiO_2 presented a mean diameter of 2.23 μm. The effluent degradation process was evaluated by photolysis and photocatalysis. In the degradation process of MB by photolysis, a maximum efficiency of 15% was obtained with the use of three irradiation intensities. In the photocatalysis process, it was observed that in pH = 10.0 and initial MB concentration of 2.0 μmol L^{-1}, the photodegradation was higher. This is due to the surface of TiO_2 particles in alkaline medium and to the presence of photocatalysts promoting the formation of hydroxyl radicals, resulting in efficiency greater than 93.0%. Therefore, the ultraviolet (UV) treatment process caused a smaller reduction in MB degradation, while the UV/TiO_2 technique was more efficient, presenting potential for this application.

Keywords: Heterogeneous photocatalysis; Titanium dioxide; Laboratory effluent; Photo degradation; Methylene blue

* Corresponding author.

1. Introduction

Environmental issues are becoming increasingly critical and frequent. Natural waters have been identified as one of the hydric resources most degraded by society. In this regard, water quality control standards and regulations against hazardous pollutants have become stricter in many countries. These effluents when not correctly treated, besides being a source of visual pollution, offer various risks of environmental impact, mainly due to the interference in the natural photosynthetic processes causing incalculable damage to all aquatic biota. The impact of these organic effluents on the environment is a big concern because of the potentially carcinogenic properties of these chemicals [1].

Jardim [2] in 1998 already pointed to a large environmental problem generated in the laboratories of universities concerning teaching and research activities. They are more complex situations due to the great diversity of the waste produced, despite the lower amount generated compared with an industrial unit. In recent years, a growing concern with the waste generated in the labs of teaching and research universities is evidenced by the increasing number of articles and books published on the subject.

Many of the effluents generated in laboratories are colored organic liquid wastes, by-products of chemical reactions and are difficult to treat. They are discarded directly into the laboratory's sinks causing negative environmental impacts [3].

The effluents containing organic compounds with different functionalities are difficult to effectively treat by classical methods, such as coagulation, flotation, sedimentation and adsorption. Furthermore, all these treatments mentioned above have a major flaw of simple transferring the pollutants from one phase to another rather than destroying them, which consequently leads to secondary pollution [4]. However, the search to improve the efficiency of the adsorption process is continuously sought through new adsorbents with special characters while performing the removal process under optimal operating conditions [5].

The numerous discoveries in nanoscience, nanotechnology and recent innovations in the field of catalytic treatment of gaseous effluents, water, sewage and soil make the heterogeneous photocatalysis allied to other treatment techniques an always-evolving subject in the environmental area [6].

Another set of techniques which are relatively new, more powerful and very promising are called advanced oxidation processes which has been developed and employed to treat dye-contaminated wastewater effluents, as heterogeneous photocatalysis [7].

The heterogeneous photocatalysis is a process where a semiconductor absorbs photons energy and acts as catalyst producing reactive radicals, mainly hydroxyl radicals. These can oxidize and mineralize organic compounds. Therefore these organic molecules are decomposed to form carbonic gas, water and mineral acids [8].

A semi-conductor is characterized by its valence and conduction bands, being the area between them called bandgap. In the photocatalysis, a semi-conductor is activated by the energy of photons absorption, which must be higher than the energy of the bandgap. This results in displacement of electrons from the valence band (BV) to the conduction band (BC), with the concomitant generation of a hole (h^+), in the valence band [9].

These holes, located in the valence band, show quite positive potentials, in the strip between 2.0 and 3.5 V. These potentials are sufficiently positive to generate radicals ($^\bullet OH$) from molecules of adsorbed water on the surface of the semi-conductor which can subsequently oxidize the organic pollutant. Electrons can migrate to the surface of the particle, where they show potentials that vary between 0.0 and –1.0 V, therefore being good reductors [10].

Photocatalytic oxidation reactions are initiated when a photon of equal or higher energy level than the band gap is absorbed by a TiO_2 catalyst, displacement an electron (e^-) from the valence band to the conduction band, simultaneously generating a positive hole (h^+) in the valence band. The mechanism of generating the radicals ($^\bullet OH$ and $^\bullet O_2^-$) (Fig. 1) is presented as follows [11]:

Methylene blue (MB) is a heterocyclic aromatic chemical compound that has application in different fields, such as biology and chemistry. It has a characteristic deep blue color in the oxidized state, but the reduced form, leucomethylene blue, is colorless [12]. In the process of degradation, the MB molecule is oxidized under the action of hydroxyl radicals formed according to reaction (b) shown in Fig. 1, with the total mineralization of this compound occurring. The objective of this study is to evaluate the photocatalytic degradation of colored effluents generated in laboratories, where MB was used as a standard compound, at two pH levels (4.0 and 10.0). Radiation intensity, photolysis and the effect of catalyst loading were examined.

2. Experimental

2.1. Chemicals

The photocatalyst employed as titanium dioxide (TiO_2) source was (P-25®) in the form of a fine powder (a mixture of two phases, 80% anatase and 20% rutile) supplied by Degussa® (Munich, Germany). It was used in this study for the effluent treatment, with molecular structure showed in Fig. 2a. MB (purity 99.5%) with molecular formula $C_{16}H_{18}N_3SCl{\cdot}3H_2O$, used as model pollutant was obtained from Merck Chemicals, (Darmstadt, Germany) without any additional purification, with molar mass 319.86 g mol^{-1}, and molecular structure shown in Fig. 2b.

$$TiO_2 + h\nu \rightarrow TiO_2(e^- + h^+) \quad \text{(a)}$$

$$H_2O + TiO_2(h^+) \rightarrow TiO_2 + {}^\bullet OH + H^+ \quad \text{(b)}$$

$$O_2 + TiO_2(e^-) \rightarrow TiO_2 + {}^\bullet O_2^- \quad \text{(c)}$$

Fig. 1. Mechanism of generating the radicals ($^\bullet OH$ and $^\bullet O_2^-$).

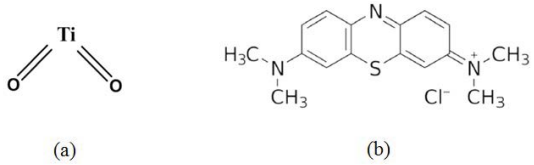

(a) (b)

Fig. 2. Molecular structure of (a) TiO_2 and (b) MB.

2.2. Characterizations of titanium dioxide

The chemical analysis of TiO_2 was performed using X-ray dispersive energy spectroscopy in the Shimadzu EDX-700HS instrument (Duisburg, Germany). X-ray diffraction (XRD) analysis for TiO_2 was conducted on a Shimadzu XRD-6000 diffractometer instrument (Tokyo, Japan), using copper Kα radiation (λ = 1.541 Å), 40 kV of voltage, current 30 mA, scanning from 2 to 75 with a scan rate of 2 min^{-1}. The analysis of Fourier transform infrared spectroscopy (FTIR) was performed on a PerkinElmer Analytical Instruments (Massachusetts, United States) Spectrum 400 spectrometer with scan from 4,000 to 400 cm^{-1}. Analysis of scanning electron microscopy (SEM) was performed on the Tescan Analytics Equipments (Brno, Czech republic), model Vega 3, operating at 20 kV. A morphological analysis of the surface of TiO_2 was performed. The material was gold sputtered on the Shimadzu IC sputter 50 equipment, using a current of 4 mA for a period of 3 min. The granulometric distribution was performed in a Mastersizer 2000 of Malvern, Instruments Ltd. (Malvern, United Kingdom). In this method, the proportional relation between laser diffraction, concentration and particle size is combined. All analyses were performed in the Materials Characterization Laboratory of the Academic Unit of Materials Engineering at the Federal University of Campina Grande.

2.3. Characterization of MB

The sweeping spectrophotometry of the MB was done in a Fenton Plus 700 spectrophotometer, with concentrations ranging between 1.0 and 6.0 μmol L^{-1}. The analysis was performed at the Environmental Science Research Laboratory of the Department of Sanitary and Environmental Engineering of Paraíba State University.

2.4. Photocatalytic process

The photocatalytic activity of a semiconductor is a result of the production of excited electrons under UV irradiation in its conduction band along with corresponding positive holes in the valence band, which react with adsorbed contaminants on the photocatalyst surface. The photocatalytic experiments were conducted under identical conditions to photolysis, but in the presence of a catalyst. The reactor consists of a cylindrical vase (Fig. 3), made with Pyrex glass with a volume of 1,000 mL, located under 3 UV lamps (254 nm wavelength; 15 W Royal Philips Electronics, Amsterdam, Netherlands). The distance between the surface of the solutions and the lamps was 0.25 m, and the total light intensity was 1.679 mW cm^{-2}. The working temperature was ~23°C (room temperature). The photocatalyst was maintained stirred and in suspension. The degradation of the MB was monitored using a Fenton Plus 700 Spectrophotometer, by assessing the intensity of the electronic absorption band located at 664 nm. The adsorption–desorption equilibrium was reached (in dark) before the photocatalytic investigation [13].

The experiments were conducted in two stages: first, with UV radiation and absence of catalysts (photolysis), in the second, with UV radiation and the presence of the catalyst (photocatalysis). The influence of the pH of the solutions, in acidic and alkaline range (4.0 and 10.0), time of radiation exposure, radiation intensity and the variation of the catalysts concentration in the MB degradation was analyzed. The samples were removed in 30 min and centrifuged at 3,200 rpm, in a Fanem Excelsa II 206BL centrifuge. Photocatalysis experiments were performed in the Environmental Sciences Research Laboratory of the Department of Sanitary and Environmental Engineering of the State University of Paraiba.

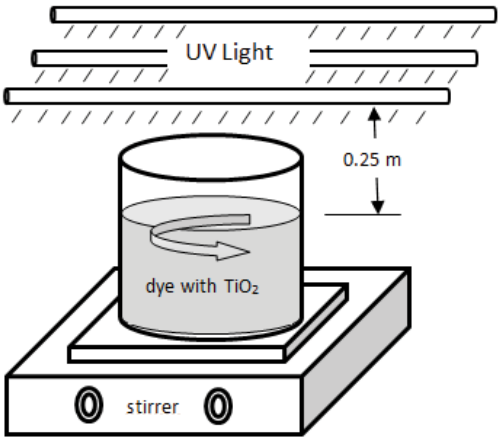

Fig. 3. Apparatus for carrying out photocatalytic studies of dye solution.

3. Results and discussion

3.1. Titanium dioxide characterization

In this topic, the characterization of the commercial TiO_2 was made. With this characterization, it will be confirmed that its chemical physical properties adjust for its use as an efficient photocatalyst.

3.1.1. X-ray fluorescence

The chemical composition of the TiO_2 was determined through X-ray fluorescence (XFR) data. Table 1 shows the chemical composition in % by weight, normalized to 100% oxides.

It could be proved that the TiO_2 presents a purity of 98.6%, with the presence of secondary mineral oxides, by using a semi-quantitative technique [14]. The data obtained corroborate with the composition of the Degussa (Munich, Germany) P25 material as described in the manufacturer's file (TiO_2 min 98%). The detection of phosphorus pentoxide by XFR is predicted by the manufacturer (0–2%) and could indicate the presence of some type of additive based on phosphate and potassium as a dispersant due to its main application as pigment. The presence of secondary oxides can accelerate or delay the transformation of anatase-rutile phase, due increase or decrease of the concentration of vacancies present in the crystalline phases of the sample.

3.1.2. X-ray diffraction

By X-ray diffraction, it was possible to identify the phases and crystal planes in the sample, as can be seen in Fig. 4.

According to the diffractogram shown in Fig. 4, it can be seen that the crystalline characteristic phases of TiO_2 were anatase and rutile. The characteristic diffraction peaks of

Table 1
TiO_2 purity and amount of impurities semiquantified

Constituent	Percentage (%)
TiO_2	98.603
Sb_2O_3	0.468
P_2O_5	0.409
K_2O	0.362
SO_3	0.101
NbO	0.034
ZrO_2	0.023

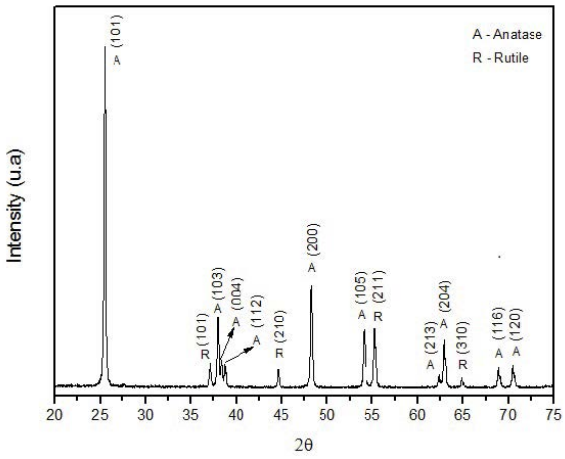

Fig. 4. Diffractogram XRD of TiO_2.

TiO_2 anatase phase are 2θ = 25.4°; 37.9°; 38.4°; 38.7°; 48.3°; 54.0°; 62.2°; 62.9°; 68.8°; 70.5° and of the crystalline planes (101), (103), (004), (112), (200), (105), (213), (204), (116) and (220), respectively. Also, in the XRD pattern, it was seen the characteristic peaks of TiO_2`s rutile phase to 2θ = 37.8°; 44.5°; 55.5°; 64.8° and crystalline planes (101), (210), (211) and (310), respectively [15]. Therefore, the samples prevailed in the anatase phase, confirming that the material used as a source of TiO_2 was Degussa (Munich, Germany) P25, which consists of 70% anatase and 30% rutile [16]. The photocatalytic activity of TiO_2 is strongly dependent on its crystallite size, phase structure, porous structure and specific surface area. Because of a larger band gap (3.2 eV) of anatase than that of rutile (3.0 eV), anatase has lower absorbance ability towards solar light. The photocatalytic activity of anatase is apparently superior than rutile. This is due to that anatase lower charge carrier recombination rate and higher surface adsorption capacity to hydroxyl groups [17]. The anatase crystalline is the greater phase. This characteristic is important because it is the most photoactive phase of titanium dioxide, which is highly desirable in photocatalytic degradation processes [18].

3.1.3. Fourier transform infrared spectroscopy

The results of the FTIR analysis of the titanium dioxide's characteristic bands can be seen in Fig. 5.

In Fig. 5 the spectrum band observed by the FTIR spectrum band, at 505 cm^{-1}, is due to the vibration of the Ti–O

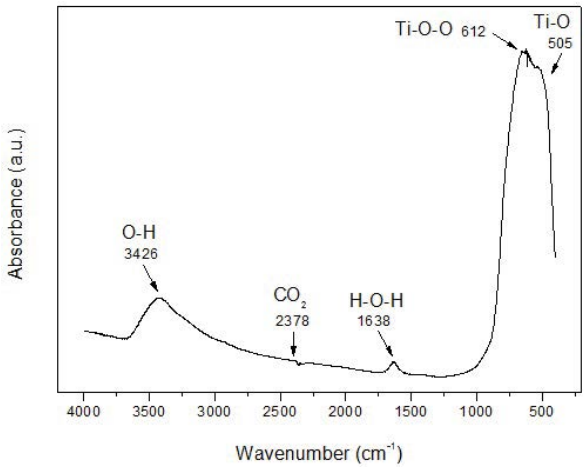

Fig. 5. FTIR spectrum of titanium dioxide.

bond [19] and the band at 612 cm^{-1} is assigned to the vibration of the Ti–O–O bond [20]. A broad peak seen in the range between 403 and 978 cm^{-1} was due to the vibrations of six coordinated TiO_6 octahedron and four coordinated Ti–O starching of anatase titania. The band at 1,638 cm^{-1} is attributed to the H–O–H bonding vibration mode of physisorbed water [21]. The band at 2,378 cm^{-1} is assigned to CO_2 present in the atmosphere [22]. For TiO_2 sample, the spectrum displays strong absorption band at 3,426 cm^{-1} corresponding to isolated –OH, related to stretching frequency of –OH attributed to the surface water adsorbed by the TiO_2 sample. The number of O–H groups adsorbed on the catalyst's surface is responsible for enhancing the photocatalytic efficiency [23].

3.1.4. Scanning electron microscopy

The SEM photomicrographs were necessary to study the microstructure of TiO_2, to identify the size, shape and power of agglomeration of the particle, as it is shown in Fig. 6.

From the photomicrographs, it can be observed in Figs. 6a and b, increased 5,000x and 10,000x, respectively, that the samples had a morphological variation over its surface, presence of large agglomerates of particles with different sizes without defined formats, with little homogeneous distribution of these aggregates. Most commercially available nanoparticles are large agglomerates about 1 μm in maximum dimension composed of primary particles with sizes ranging from 5 to 50 nm. The large agglomerates scatter light and are not directly suitable for optical systems [24]. The primary particles can be held together by weak Van der Waals interactions in the case of clusters or by strong interactions in the case of aggregates. The degree of agglomeration of TiO_2 particles depends on factors such as suspension pH, ionic strength, particle size and particle concentration [25].

In Figs. 6c and d, with larger increases of 15,000x and 20,000x, respectively, it was observed morphological structure on microscale particles of spherical form, uniformly distributed [26]. The microstructure of the TiO_2 particles founded, favors their application in the photocatalytic

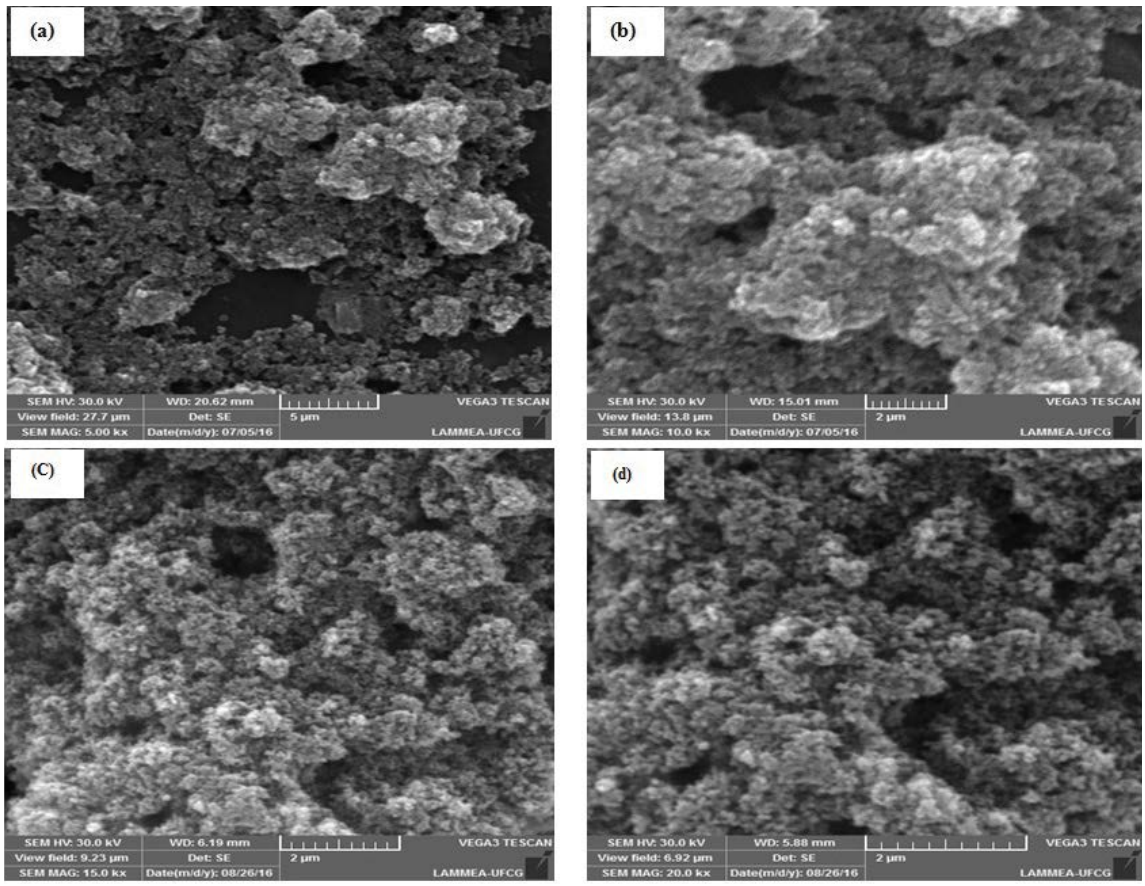

Fig. 6. Titanium dioxide SEM photomicrographs with increases of: (a) 5,000x, (b) 10,000x, (c) 15,000x and (d) 20,000x.

process, because many factors have a significant influence on the performance, including the size, specific surface area, pore volume, pore structure, crystal phase and aspects of the exposed surface [27].

3.1.5. Granulometric distribution

Fig. 7 shows the granulometric distribution and the particles mean diameter of TiO_2.

The particle size distribution is bimodal with a distribution band of 2.23 µm mean particle diameter. The size distribution range extends from 0.04 to about 10 µm, and about 57.35% mass of the accumulated particles present size smaller than 2 µm. The narrower the distribution presented by the particle diameter curve, the greater the homogeneity regarding the distribution, size and geometry of the particles. In addition, d_{10} = 10% of the particles with diameters smaller than 0.15 µm, d_{50} = 50% of the particles with diameters smaller than 1.57 µm and d_{90} = 90% of the particles with diameters smaller than 5.64 µm [28]. The decrease in particle size is accompanied by an increase in the surface/volume ratio, which causes the surface energy to contribute significantly to the total energy of the material. This means that for particles of reduced size, the polymorphic form with lower surface energy exhibits the highest thermodynamic stability, which contributes to a better performance of the photocatalytic process [29].

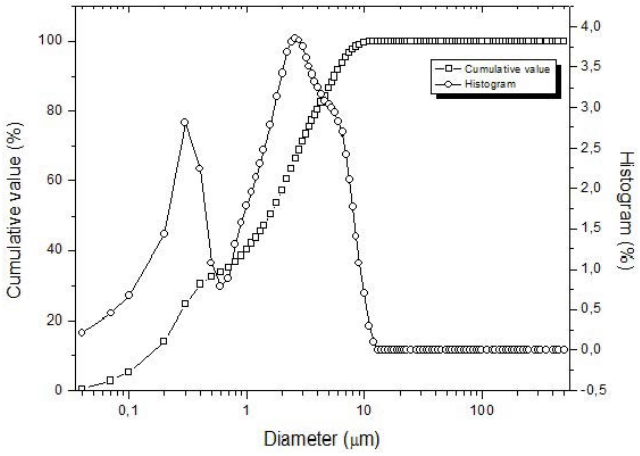

Fig. 7. Granulometric distribution of TiO_2.

3.2. Methylene blue characterization

The sweeping spectrophotometry of the MB was done in a Fenton Plus 700 spectrophotometer (Fig. 8), for concentrations ranging between 1.0 and 6.0 µmol L^{-1}. Maximum absorbance occurred at a 660 nm wavelength, independent of the concentration [30].

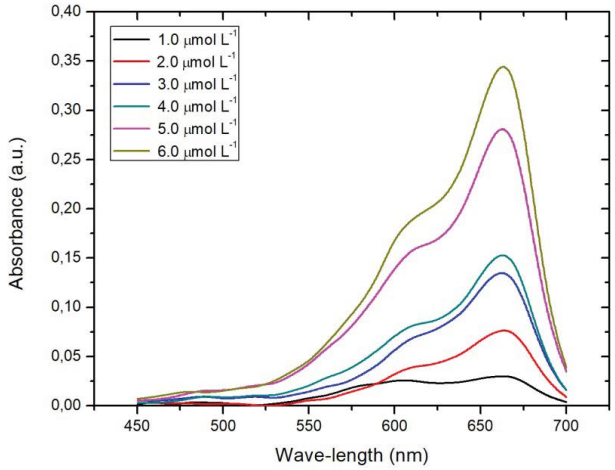

Fig. 8. Molecular absorption spectrum of MB.

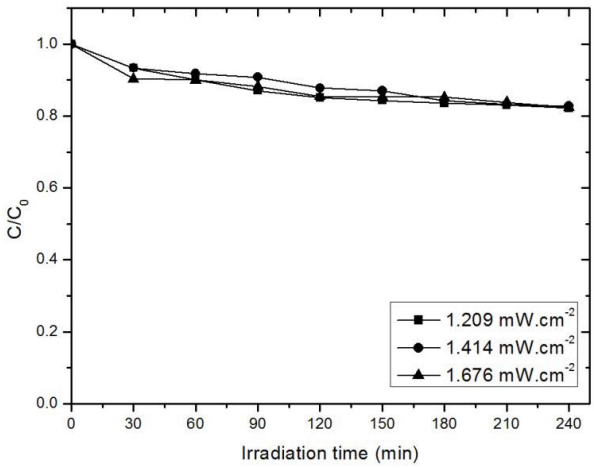

Fig. 9. Photolysis in the degradation of MB.

3.3. Photocatalytic and photolysis process

The degradation of MB by illumination, under the same conditions, can be detected as a standard measure of a sample's photocatalytic activity in which MB aqueous solution is used to simulate an organic pollutant.

3.3.1. Determination of concentration of dye decomposition

The determination of the concentration of dye can be described by the Beer–Lambert Law. When a monochromatic light beam passes through the solution, the amount of light absorbed by the solution is directly related to its concentration according to Eq. (1).

$$A = \epsilon bc \quad (1)$$

where A is the absorbed light, ε is the absorption coefficient, b is the solution thickness and c is the dye concentration solution at sampling time [31]. According to the Beer–Lambert Law, the relationship between dye concentration and absorbed light is linear. The measurements for determining dye concentration were done at an interval where its relationship is still linear.

3.3.1. Effect of the radiation intensity in the photolysis process

Fig. 9 shows the effect of the radiation intensity on the photolysis process of the MB degradation, irradiated for 4 h. According to the obtained data, it was possible to observe that the photolysis was not efficient for degradation of the MB. Three different intensities of irradiation were used, reaching degradation of 15%, leading to the need of photocatalysis with TiO_2 for the total degradation [32].

3.3.2. Effect of the initial pH and initial MB concentration on the degradation rates

One of the most important parameters that influence the photocatalytic degradation of dye is the pH. This is due to the effect of pH on the charge properties of the surface of the photocatalyst and to the influences on the ionic species in the

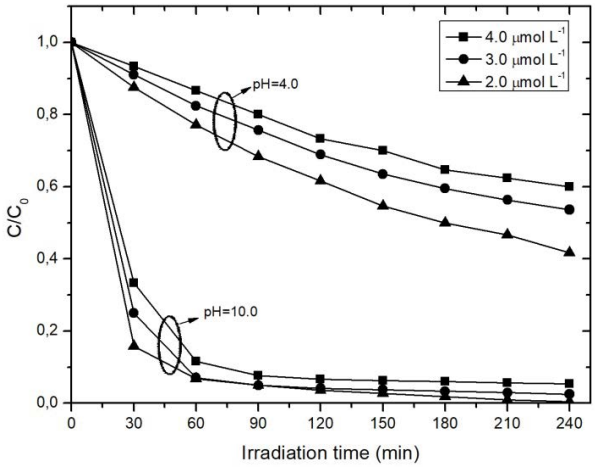

Fig. 10. Effect of the initial pH and initial MB concentration on the degradation rates.

solution [33]. Therefore, the effects of pH were investigated in the photocatalytic activity of MB. Different experiments were carried out with pH values of 4.0 and 10.0, as shown in Fig. 10. The concentration of MB was variable (2.0, 3.0 and 4.0 μmol L^{-1}) and dose of catalyst was fixed at 3.0 g L^{-1}. Before illumination, the suspensions were shaken in the dark for 60 min to achieve an adsorption–desorption equilibrium between the photocatalyst and the MB. Then, the suspensions were exposed to irradiation for additional 240 min. The experiments were performed at the same time. It is possible to observe that the degradation increases with the increase of pH. The best degradation was observed in pH = 10 reaching 95% in 90 min of operation. For pH = 4.0 the maximum degradation was 57%, achieved in 240 min. The influence of pH on the degradation rate of organic dyes is variable and controversial, because in some cases degradation occurs better in acidic pH [34] and in others in alkaline pH [35]. The pH variation changes the charge on the surface of the TiO_2 particles and the potential of the catalyst reactions varies. With the variation of the potential, the adsorption of the dye on the

surface of the catalyst varies and as a result causes variation in the speed of the reaction.

Under acidic and alkaline surface conditions, TiO_2 can be pseudo-proton and/or negatively charged, respectively. MB is a cationic dye, and the surface of the TiO_2 particles in the alkaline media obtain negative charges, so the cationic types can be readily absorbed. Thus, photodegradation is best done under the alkaline conditions [36].

It is still possible to verify in Fig. 10 the effect of the initial concentration of MB according to the exposure time of the photocatalytic process (UV/TiO_2). The degradation efficiency of MB was more effective at low concentrations. This can be better observed at pH = 4.0, for the initial concentration of 2.0 μmol L^{-1}, there was a degradation rate of 58.10%, while for 3.0 and 4.0 μmol L^{-1} was 46.44% and 40.19%, respectively, in approximately 240 min. At pH = 10.0 the effect of the initial concentration of the dye was not significant but followed the trend of pH = 4.0, where there was a better degradation at lower concentrations, reaching 99.0% in 240 min. In this case, the more concentrated solutions will absorb the UV radiation, competing with the photocatalyst (TiO_2) and, consequently, fewer photons will absorb the photocatalyst to generate hydroxyl radicals to promote the reactions [37].

3.3.3. Photolytic and photocatalytic processes efficiency

In photolysis, the water molecule was cleaved, under UV light, in hydrogen and hydroxyl radicals [38]. In photocatalysis, as UV light activates the TiO_2, holes and electrons are generated in the valence band (VB) and the conduction band (CB). Since most semiconductors consist of nanocrystalline solids, electron/gap charges can migrate to the particle surface. Holes in VB oxidize hydroxyl groups and water forming hydroxyl and peroxide radicals. The radicals decompose the dehydrated organic molecules until final non-toxic products [39].

Fig. 11 shows the data obtained for the photolysis and photocatalysis process (pH = 10.0, TiO_2 loading of 3.0 g L^{-1} and varying concentrations of MB). It is observed that in the photocatalysis process, degradation is higher for any initial concentration of the dye, because in the presence of the photocatalysts the formation of hydroxyl radicals occurs, which leads to degradation of the MB.

3.4. Calculation of the degradation efficiency, η

The degradation efficiency (η) of MB at a reaction time *t* (min) was calculated as follows:

$$\eta = \frac{C_0 - C}{C_0} \times 100\% \tag{2}$$

where C_0 is the initial MB concentration (μmol L^{-1}) and *C* is the MB concentration (μmol L^{-1}) at a reaction time *t* (min). The values are reported in Table 2.

3.5. Kinetic analysis of photocatalytic degradation

The photocatalytic degradation of MB obeys the pseudo-first-order of kinetic in terms of modified Langmuir–Hinshelwood (L–H) model by Eq. (3):

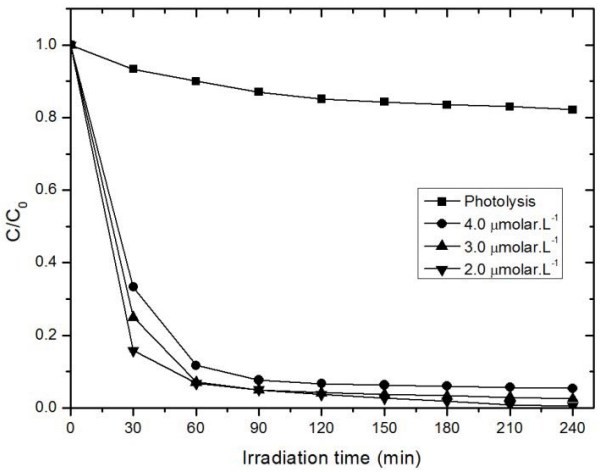

Fig. 11. Photolytic and photocatalytic processes efficiency.

$$r = -\frac{dC}{dt} = \frac{k_r \cdot k_a \cdot C}{1 + k_a \cdot C} \tag{3}$$

In this equation, *r* (μmol L^{-1} min^{-1}), k_r (μmol L^{-1} min^{-1}), k_a (L μmol^{-1}), *C* (L μmol^{-1}) and *t* (min) are the reaction rate, reaction rate constant, adsorption constant, reactant concentration and time of irradiation, respectively [13,40–42]. At low initial dye concentration, the rate expression (Eq. (1)) can be written in the form of Eq. (4):

$$r = -\frac{dC}{dt} = k_r \cdot k_a \cdot C = k \cdot C \tag{4}$$

where *k* is the pseudo-first-order rate constant and by integration of Eq. (3) with the limit of $C = C_0$ at $t = 0$, it changes to Eq. (5):

$$ln\left(\frac{C}{C_0}\right) = -k \cdot t \tag{5}$$

In Eq. (5), C_0 is the initial concentration and *C* is the sum of the dye solution concentrations at each moment. According to Eq. (5), the plot of $ln(C/C_0)$ vs. *t* for all concentrations should be linear and the values of *k* can be obtained directly via its slope. One of the most useful indications to evaluate the reaction rate of first order kinetics is the calculation of half-life time reaction. The half-life ($t_{1/2}$) was calculated by Eq. (6) as follows:

$$t_{1/2} = \frac{\ln(2)}{k} \tag{6}$$

Figs. 12 and 13 show the ln (C/C_0) as a function of time and represent a straight line. The slope of the linear regression is equal to the apparent first order rate constant *k*. Their corresponding values for two pH levels (4.0 and 10.0) and different initial concentrations are regrouped in Table 2.

The photocatalytic degradation of organic compounds typically follows first-order kinetics. However, the rate of reaction varies with the complexity of degradation, the

Table 2
Kinetic parameters in the degradation of MB following a photocatalytic reaction

pH	C_0 (μmol L^{-1})	C_f (μmol L^{-1})	η (%)	Stage	K (min^{-1})	$t_{½}$ (min)	R^2
4.0	4.0	2.3924	40.19	1	0.0023	301.36	0.99552
	3.0	1.6068	46.44	1	0.0028	247.55	0.99484
	2.0	0.8318	58.10	1	0.0038	182.41	0.99677
10.0	4.0	0.4584	88.54	1	0.03597	19.27	0.99988
	3.0	0.2331	92.23	1	0.04454	15.56	0.99947
	2.0	0.1274	93.63	1	0.04824	14.36	0.97189
	0.4584	0.0239	94.78	2	0.00364	190.42	0.75636
	0.2331	0.0062	97.33	2	0.00527	131.52	0.94898
	0.1274	0.0009	99.30	2	0.01456	47.61	0.95312

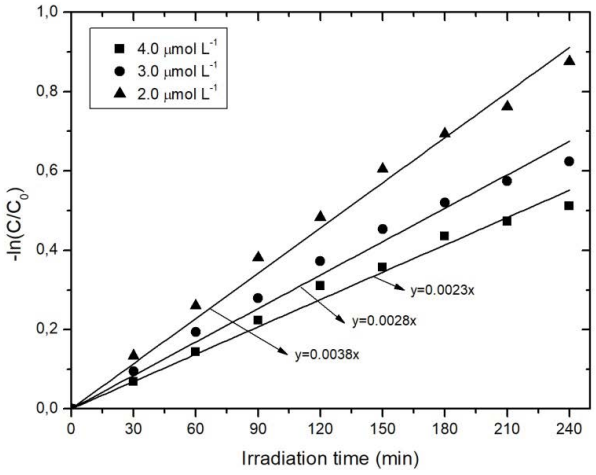

Fig. 12. Linear transformation $ln(C/C_0) = f(t)$ of the disappearance of MB (pH = 4.0, TiO_2 concentration = 0.3 mg L^{-1}).

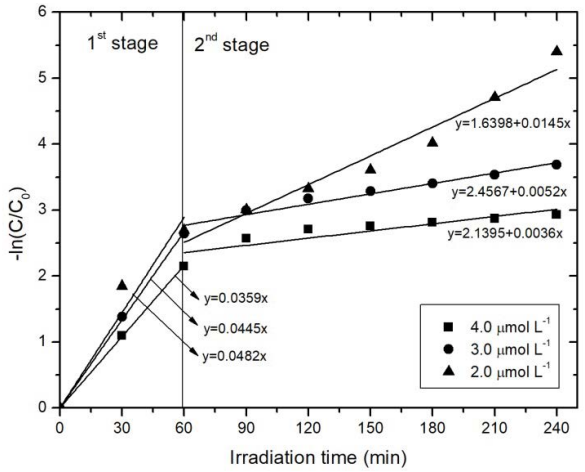

Fig. 13. Linear transformation $ln(C/C_0) = f(t)$ of the degradation of MB (pH = 10.0, TiO_2 concentration = 0.3 mg L^{-1}).

amount of substrate adsorbed onto the surface of the catalyst, and the absorption spectra of the substrate. When substrates with high UV absorption coefficients are used in excess, they cover the surface of the catalyst and prevent the penetration of radiation [43].

In the present study, when the pH level was 4.0 with initial concentration of (4.0, 3.0 and 2.0 μmol L^{-1}) MB, the degradation process was slow and incomplete (240 min; Fig. 12). For the level of pH = 10.0, for the same concentrations of the substrate, the photocatalysis occurred in two distinct stages, the first faster (60 min) and the second much slower (60–240 min; Fig. 13). A similar dependence was also observed during the photodegradation of Bisphenol A and diclofenac [44].

Table 2 lists the first order apparent rate constants (k) for different pH levels, which were calculated from Figs. 12 and 13. For the pH = 4.0 the values obtained for k are equal to 0.0023, 0.0028 and 0.0038 min^{-1} for initial concentrations of 4.0, 3.0 and 2.0 μmol L^{-1}, respectively. Therefore, the initial concentration of MB has a significant effect on the degradation rates, since the constant rate of degradation is higher when the initial concentration is lower.

For pH = 10.0, the degradation reaction occurs in two stages, one rapid (1 stage) between 0 and 60 min and another slow (2 stages) between 60 and 240 min. For the first stage the values obtained for k are equal to 0.03597, 0.04454 and 0.04824 min^{-1} for initial concentrations of 4.0, 3.0 and 2.0 μmol L^{-1}, respectively. In the second stage, the values obtained for k are 0.00364, 0.00527 and 0.01456 min^{-1} for the initial stage concentrations of 0.4584, 0.2331 and 0.1274 μmol L^{-1}, respectively. Again showing that the initial concentration of MB has a significant effect on degradation rates, since the constant rate of degradation is higher when the initial concentration is lower.

Linear regressions for pH = 4.0 were R^2 = 0.9955, R^2 = 0.9948, R^2 = 0.9967, respectively, for the above concentrations. While for pH = 10.0 the regressions for the first stage were R^2 = 0.9998, R^2 = 0.9994, R^2 = 0.9718 and second stage were R^2 = 0.7564, R^2 = 0.9489, R^2 = 0.9531, respectively. This clearly indicates that the MB photodegradation reaction obeys a first order kinetics.

4. Conclusion

The TiO_2 analyzes by XFR, XRD, SEM and granulometry presented composition, predominant anatase crystalline structure and particles size suitable for application in photocatalytic processes. It was observed significant differences in degradation using the photolysis and photocatalysis process

(UV/TiO_2). The photolysis did not present satisfying results when compared with the photocatalysis, in the studied pH levels. In photocatalytic process, the degradation of methylene blue in different concentrations and pH values, showed that MB degradation was very efficient, with an average value of 94.33% at pH 10, this efficiency drops to 48.24% at pH 4.0, for the lowest initial dye concentration. In addition, the calculated process kinetics indicated that MB degradation can be divided into two stages, one faster up to 60 min and one slower between 60 and 240 min. Therefore, UV/TiO_2 photocatalysis could be used as a promising process for MB photodegradation.

Acknowledgments

The authors appreciate the PIBIC/UEPB/CNPq, Materials Characterization Laboratory in UFCG and the Environmental Sciences Research Laboratory in UEPB for their financial support.

References

[1] M.A. Rauf, M.A. Meetani, A. Khaleel, A. Ahmed, Photocatalytic degradation of Methylene Blue using a mixed catalyst and product analysis by LC/MS, Chem. Eng. J., 157 (2010) 373–378.
[2] W.F. Jardim, Chemical waste management in teaching and research laboratories, New Chem., 21 (1998) 671–675.
[3] E.S. Nascimento, A.T. Filho, Chemical waste risk reduction and environmental impact generated by laboratory activities in research and teaching institutions, Braz. J. Pharm. Sci., 46 (2010) 187–198.
[4] D. Zhang, F. Zeng, Visible light-activated cadmium-doped ZnO nanostructured photocatalyst for the treatment of methylene blue dye, J. Mater. Sci., 47 (2012) 2155–2161.
[5] N.B. Swan, M.A.A. Zaini, Adsorption of malachite green and congo red dyes from water: recent progress and future outlook, Ecol. Chem. Eng. S, 26 (2019) 119–132.
[6] S. Wacławek, V.V.T. Padil, M. Černík, Major advances and challenges in heterogeneous catalysis for environmental applications: a review, Ecol. Chem. Eng. S, 25 (2018) 9–34.
[7] M. Muruganandham, R.P.S. Suri, S.H. Jafari, M. Sillanpää, G.J. Lee, J.J. Wu, M. Swaminathan, Recent developments in homogeneous advanced oxidation processes for water and wastewater treatment, Int. J. Photoenergy, 2014 (2014) 1–21.
[8] D. Bahnemann, Photocatalytic water treatment: solar energy applications, Sol. Energy, 77 (2004) 445–459.
[9] G.G. Bessegato, T.T. Guaraldo, J.F. Brito, M.F. Brugnera, M.V.B. Zanoni, Achievements and trends in photoelectrocatalysis: from environmental to energy applications, Electrocatalysis, 2015 (2015) 1–27.
[10] D. Friedmann, A. Hakki, H. Kim, W. Choic, D. Bahnemannd, Heterogeneous photocatalytic organic synthesis: state of the art and future perspectives, Green Chem., 18 (2016) 5391–5411.
[11] M. Muneer, B. Abbad, A.A.H. Kadhum, A.B. Mohamad, M.S. Takriff, K. Sopian, Synthesis and catalytic activity of TiO_2 nanoparticles for photochemical oxidation of concentrated chlorophenols under direct solar radiation, Int. J. Electrochem. Sci., 7 (2012) 4871–4888.
[12] F. Kazemi, Z. Mohamadnia, B. Kaboudin, Z. Karimi, Photodegradation of methylene blue with a titanium dioxide/polyacrylamide photocatalyst under sunlight, J. Appl. Polym. Sci., 43386 (2016) 1–9.
[13] T. Soltani, M.H. Entezari, Photolysis and photocatalysis of methylene blue by ferrite bismuth nanoparticles under sunlight irradiation, J. Mol. Catal., A, 377 (2013) 197–203.
[14] A.G.S. Galdino, E.M. Oliveira, F.B.F. Monteiro, C.A.C. Zavaglia, In vitro assay analysis of the 50% HA-50% TiO_2 composite manufactured by the polymeric sponge method, Ceramics, 60 (2014) 586–593.
[15] A. Matioli, J. Miagava, D. Gouvêa, Modification of stability of nanometric TiO_2 polymorphs by SnO_2 surface excess, Ceramics, 58 (2012) 53–57.
[16] C.C. Moro, M.A. Lansarin, M. Bagnara, Nitrogen doped TiO_2 nanotubes: comparison of photocatalytic activities of materials obtained by different techniques, New Chem., 35 (2012) 1560–1565.
[17] S. Sohrabnezhad, Study of catalytic reduction and photodegradation of methylene blue by heterogeneous catalyst, Spectrochim. Acta, Part A, 81 (2011) 228–235.
[18] G.T. Saleiro, S.L. Cardoso, R. Toledo, J.N.F. Holanda, Evaluation of the crystalline phases of red ceramic supported titanium dioxide, Ceramics, 56 (2010) 162–167.
[19] B. Choudhury, A. Choudhury, Luminescence characteristics of cobalt doped TiO_2 nanoparticles, J. Lumin., 132 (2012) 178–184.
[20] L.G. Devi, B.N. Murhty, S.G. Kumar, Photocatalytic degradation of imidachloprid under solar light using metal ion doped TiO_2 nano particles: influence of oxidation state and electronic configuration of dopants, Catal. Lett., 130 (2009) 496–503.
[21] V.G. Gandhi, M.K. Mishra, P.A. Joshi, A study on deactivation and regeneration of titanium dioxide during photocatalytic degradation of phthalic acid, J. Ind. Eng. Chem., 18 (2012) 1902–1907.
[22] T. Venkov, K. Hadjiivanov, FTIR study of CO interaction with Cu/TiO_2, Catal. Commun., 4 (2003) 209–213.
[23] A.D. Vishwanath, J.S. Shankar, N.M. Eknath, A.A. Eknath, K.N. Haribhau, Preparation, characterization and photocatalytic activities of TiO_2 towards methyl red degradation, Orient. J. Chem. 33 (2017) 104–112.
[24] N. Mandzy, E. Grulke, T. Druffel, Breakage of TiO_2 agglomerates in electrostatically stabilized aqueous dispersions, Powder Technol., 160 (2005) 121–126.
[25] Ö.Ç. Duvarci, M. Çiftçioğlu, Preparation and characterization of nanocrystalline titania powders by sonochemical synthesis, Powder Technol., 228 (2012) 231–240.
[26] S. Joseph, B. Mathew, Microwave assisted biosynthesis of silver nanoparticles using the Rhizome extract of *Alpinia galanga* and evaluation of their catalytic and antimicrobial activities, J. Nanopart., 2014 (2014) 1–9.
[27] K. Dai, H. Chen, T. Peng, D. Ke, H. Yi, Photocatalytic degradation of methyl orange in aqueous suspension of mesoporous titania nanoparticles, Chemosphere, 69 (2007) 1361–1367.
[28] I. Ayadi, F.B. Ayed, Sintering and the mechanical properties of the tricalcium phosphate–titania composites, J. Mech. Behav. Biomed. Mater., 49 (2015) 129–140.
[29] G. Li, L. Lv, H. Fan, J. Ma, Y. Li, Y. Wan, X.S. Zhao, Effect of the agglomeration of TiO_2 nanoparticles on their photocatalytic performance in the aqueous phase, J. Colloid Interface Sci., 348 (2010) 342–347.
[30] F. Liu, R. Jamal, Y. Wang, M. Wang, L. Yang, T. Abdiryim, Photodegradation of methylene blue by photocatalyst of D-A-D type polymer/functionalized multi-walled carbon nanotubes composite under visible-light irradiation, Chemosphere, 168 (2017) 1669–1676.
[31] Y. Chihiro, K. Kazuo, W. Noriyuki, T. Hiroshi, T. Tomoo, M. Tadashi, T. Hitoshi, Photocatalytic degradation of methylene blue by TiO_2 film and Au particles-TiO_2 composite film, Thin Solid Films, 516 (2008) 5881–5884.
[32] T.M.L. Maya, M.J.L. Guzmán, R.L. Hinojosa, R.A. Hernández, Synthesis and photocatalytic activity of ZnO-CuPc for methylene blue and potassium cyanide degradation, Mater. Sci. Semicond. Process, 77 (2018) 74–82.
[33] R.S. Dariani, A. Esmaeili, A. Mortezaali, S. Dehghanpour, Photocatalytic reaction and degradation of methylene blue on TiO_2 nano-sized particles, Optik, 127 (2016) 7143–7154.
[34] M.A. Habib, I.M.I. Ismail, A.J. Mahmood, M.R. Ullah, Photocatalytic decolorization of Brilliant Golden Yellow in TiO_2 and ZnO suspensions, J. Saudi Chem. Soc., 16 (2012) 423–429.
[35] A.H. Jawad, N.S.A. Mubarak, M.A.M. Ishak, K. Ismail, W.I. Nawawi, Kinetics of photocatalytic decolourization of cationic dye using porous TiO_2 film, J. Taibah Univ. Sci., 10 (2016) 352–362.

[36] M.R. Khan, A.S.W. Kurny, G. Fahmida, Parameters affecting the photocatalytic degradation of dyes using TiO_2: a review, Appl. Water Sci., 7 (2017) 1569–1578.
[37] K. Soutsas, V. Karayannis, I. Poulios, A. Riga, K. Ntampegliotis, X. Spiliotis, G. Papapolymerou, Decolorization and degradation of reactive azo dyes via heterogeneous photocatalytic processes, Desalination, 250 (2010) 345–350.
[38] S. Papoutsakis, S.M. Cuevas, N. Gondrexon, S. Baup, S. Malato, C. Pulgarin, Coupling between high-frequency ultrasound and solar photo-Fenton at pilot scale for the treatment of organic contaminants: an initial approach, Ultrason. Sonochem., 22 (2012) 527–534.
[39] P. Anca, M.C. Anca, C. Nicula, L.M. Cozmuta, A. Jastrzębska, A. Olszyna, L. Baia, UV light-assisted degradation of methyl orange, methylene blue, phenol, salicylic acid, and Rhodamine B: photolysis versus photocatalyis, Water Air Soil Pollut., 228 (2017) 28–41.
[40] M. Sanchez, M.J. Rivero, I. Ortiz, Kinetics of dodecylbenzenesulphonate mineralisation by TiO_2 photocatalysis, Appl. Catal., B, 101 (2011) 515–521.
[41] J.P.S. Valente, P.M. Padilha, A.O. Florentino, Studies on the adsorption and kinetics of photodegradation of a model compound for heterogeneous photocatalysis onto TiO_2, Chemosphere, 64 (2006) 1128–1133.
[42] D. Ljubas, G. Smoljani, H. Jureti, Degradation of Methyl Orange and Congo Red dyes by using TiO_2 nanoparticles activated by the solar and the solar-like radiation, J. Environ. Manage., 161 (2015) 83–91.
[43] W.S. Lopes, M.G.C. Azevedo, V.D. Leite, J.T. Sousa, J.S. Buriti, Degradation of 17α-ethinylestradiol in water by heterogeneous photocatalysis, Environ. Water - Inter. J. Appl. Sci., 10 (2015) 728–736.
[44] E. Kudlek, D. Silvestri, S. Wacławek, V.V.T. Padil, M. Stuchlík, L. Voleský, P. Kejzlar, M. Černík, TiO_2 immobilised on biopolymer nanofibers for the removal of bisphenol A and diclofenac from water, Ecol. Chem. Eng. S, 24 (2017) 417–429.